Available online at www.sciencedirect.com
ScienceDirect
Journal of Nuclear Materials 366 (2007) 198–205
journal of nuclear materials
www.elsevier.com/locate/jnucmat

Some new experimental results on the Zr–Nb–Fe system

C. Ramos [a,*], C. Saragovi [a], M.S. Granovsky [b]

[a] Departamento de Física – CAC – Comisión Nacional de Energía Atómica, Av. Gral Paz 1499, (1650) San Martín, Buenos Aires, Argentina
[b] Departamento de Materiales – CAC – Comisión Nacional de Energía Atómica, Av. Gral Paz 1499, (1650) San Martín, Buenos Aires, Argentina

Received 1 August 2006; accepted 11 January 2007

Abstract

The scope of this study is the identification and characterization of intermetallic phases and their binary and ternary fields in the Zr–Nb–Fe phase diagram. A construction of the central region of the phase diagram at 900 °C was proposed using new experimental results obtained by optical and scanning electron microscopies, X-ray diffraction and microprobe analysis. In addition to the well-known Laves C15-type $(ZrNb)Fe_2$ phase (the polytypic C14 and C36 structures were not detected in the studied compositions), another Laves C14-type phase was found ($Zr(NbFe)_2$). Watson and Bennett maps helped to predict the occurrence of both of these phases. Moreover, the validity of the Pettifor prediction model for Laves phases in pseudobinary systems with transition elements was checked, verifying the obtained experimental results in the Zr–Nb–Fe system. On the other hand it was determined that the Zr–Nb–Fe ternary system at 900 °C, as it happens in the binary Zr–Nb system, would have a miscibility gap (β-Zr + β-Nb) in the 25–70 at.% Nb composition range, accepting up to 3 at.% Fe approximately.

PACS: 81.30.Bx

1. Introduction

Materials used in nuclear reactors should have an optimal efficiency in service, that is why it is important the knowledge of their properties like their response to thermomechanical solicitation and to corrosion. With the aim of understanding and trying to improve these properties it is fundamental to know the associated phase diagrams and the phase transformations involved in them.

Zr alloys are widely used as corrosion resistant structural materials in nuclear power reactors. Zr is particularly useful because of easy availability, good ductility, radiation damage resistance, low thermal neutron capture cross section and excellent corrosion resistance. There have been several attempts to develop new materials to be used at higher temperatures in nuclear power reactors improving the corrosion properties and the strength of Zr by alloying it with transition metals (Nb, Cr, Fe, Cu, etc.). Between them ZIRLO™[1] (Zr alloyed

* Corresponding author. Member of the Consejo Nacional de Investigaciones Científicas y Técnicas, Argentina. Tel.: +54 11 6772 7160; fax: +54 11 6772 7362.
E-mail address: ciramos@cnea.gov.ar (C. Ramos).

[1] Trademark of Westinghouse Electric Company, Pittsburgh, PA.

0022-3115/$ - see front matter © 2007 Elsevier B.V. All rights reserved.
doi:10.1016/j.jnucmat.2007.01.216

with niobium, tin and iron) is being investigated as a suitable material to be used in commercial nuclear light water reactors. Considering that this material presents Zr–Nb–Fe precipitates it is then of interest to study the ternary phase diagram corresponding to those precipitates.

In the Zr–Nb–Fe system, in addition to the phases coming from the corresponding binary systems it is important to characterize the ternary phases. One of the ternary phases found in the present work is a cubic Ti_2Ni-type phase, $(ZrNb)_2Fe$ [1–6], another one is a hexagonal C14 Laves $Zr(NbFe)_2$ phase [2–7] and the last one a cubic C15 Laves phase, $(ZrNb)Fe_2$. The latter is a polytypic phase which presents cubic C15 [2,4,8], hexagonal C36 [2] and hexagonal C14-type [2,8] structures depending on the composition. These structures occur on the $ZrFe_2$–$NbFe_2$ line of the Zr–Nb–Fe phase diagram [6].

The purpose of the present work is to determine the existence range of the ternary phases and the limits between the two-phase and the three-phase regions where these phases belong. Zr–Nb–Fe alloys with Nb contents between 5 and 50 at.% and Fe contents between 9 and 65 at.% were melted and analyzed both, as cast and heat treated at 900 °C during 2880 h. After the heat-treatment samples were water quenched to room temperature.

The determination and characterization of the phases were made by optical and scanning electron microscopies, X-ray diffraction, and microprobe analysis. Results obtained by Mössbauer spectroscopy on these samples have been recently published [9].

2. Experimental procedures

Nominal chemical compositions of the alloy samples are given in Table 1. These alloys were produced in an arc furnace with a non-consumable tungsten electrode in a high purity argon atmosphere. Between four to five remeltings were necessary to achieve a satisfactory chemical homogeneity. Starting materials were 99.9 wt% pure Fe, 99.8 wt% pure Zr and Nb and Zr–20 wt% Nb with Fe impurities less than 500 ppm and O impurities less than 1200 ppm.

Table 1
Nominal chemical compositions of the alloy samples in at.%

Zr (at.%)	30	45	40	40	40	40	61
Nb (at.%)	5	10	20	30	40	50	30
Fe (at.%)	65	45	40	30	20	10	9

Samples were heat-treated at 900 °C during 2880 h. For that purpose they were wrapped in Ta foils and then sealed in a quartz tube under a high purity argon atmosphere. After the heat-treatment the quartz tube was quenched in cold water, without breaking it, with a cooling rate of about 30 °C/s [10].

Metallographic analysis samples were ground on silicon carbide paper then polished with diamond paste (1 μm and 6 μm) and finally chemically etched by using suitable mixes of HF and HNO_3 acids for each one of the samples.

Energy dispersive spectroscopy (EDS) was performed using a Philips scanning electron microscope with an EDAX spectrometer.

Random powder samples were prepared to carry out a phase-structural characterization of the alloys by X-ray diffraction (XRD) analysis. Patterns were obtained with a Philips PW diffractometer equipped with monochromator. Measurements were performed at a speed of 0.03°/15 s in the 10–120° range using a Cu anticathode at room temperature. The obtained patterns were fitted using a Rietveld structure refinement software [11] to determine the lattice parameters.

By means of wavelength dispersive electron-probe analysis the composition of each one of the phases present in the samples was determined. This analysis was accomplished using a Cameca SX50 electron probe microanalyser operated at 20 kV with an electron beam current of 50 nA. Comparison was made through high purity Zr, Nb and Fe standards.

3. Results

The results obtained from the analysis of the samples with XRD and microanalysis techniques are summarized in Table 2. Two solid solutions (β-Zr and β-Nb), two Laves phases ($Zr(NbFe)_2$ and $(ZrNb)Fe_2$) and the $(ZrNb)_2Fe$ intermetallic appeared in the composition range studied in the present work. From now on the $(ZrNb)_2Fe$ phase will be referred as λ_1 phase and the $Zr(NbFe)_2$ phase as λ_2 phase to be consistent with [4].

The corresponding as cast samples, used as witnesses, present the same phases as the heat-treated samples in all of the cases. However the average composition of the phases in the as cast samples measured by microanalysis deviate from those of the heat-treated samples showing that in the as cast samples the phases are off-equilibrium. The lattice

Table 2
Results obtained by XRD and microprobe analysis for the heat-treated studied samples

Sample	Crystalline structure				Average composition (at.%)			Phase
	System	Type	a (nm)	c (nm)	Zr	Nb	Fe	
$Zr_{30}Nb_5Fe_{65}$	Hexagonal	$MgZn_2$	0.5083	0.8315	36.0	7.4	56.6	λ_2
	Cubic	$MgCu_2$	0.7029	–	25.1	5.3	69.6	$(ZrNb)Fe_2$
	Tetragonal	Al_2Cu	0.6409	0.5593	–	–	–	Zr_2Fe
$Zr_{45}Nb_{10}Fe_{45}$	Cubic	Ti_2Ni	1.2151	–	58.1	8.3	33.6	λ_1
	Hexagonal	$MgZn_2$	0.5109	0.8332	34.3	10.0	55.7	λ_2
$Zr_{40}Nb_{20}Fe_{40}$	Cubic	Ti_2Ni	1.2155	–	53.8	10.9	35.3	λ_1
	Hexagonal	$MgZn_2$	0.5233	0.8510	34.3	20.7	45.0	λ_2
$Zr_{40}Nb_{30}Fe_{30}$	Cubic	Ti_2Ni	1.2149	–	55.2	15.3	29.5	λ_1
	Hexagonal	$MgZn_2$	0.5320	0.8664	37.3	32.0	30.7	λ_2
	Cubic	W	0.3500	–	73.3	23.8	2.9	β-Zr
$Zr_{40}Nb_{40}Fe_{20}$	Hexagonal	$MgZn_2$	0.5342	0.8665	37.0	35.1	27.9	λ_2
	Cubic	W	0.3455	–	55.8	42.0	2.2	β-Zr
	Cubic	W	0.3360	–	21.4	77.1	1.5	β-Nb
$Zr_{40}Nb_{50}Fe_{10}$	Hexagonal	$MgZn_2$	0.5344	0.8663	34.9	35.1	30.0	λ_2
	Cubic	W	0.3449	–	49.3	47.5	3.2	β-Zr
	Cubic	W	0.3363	–	23.9	74.8	1.3	β-Nb
$Zr_{61}Nb_{30}Fe_9$	Hexagonal	$MgZn_2$	0.5335	0.8661	37.6	34.1	28.3	λ_2
	Cubic	W	0.3499	–	67.7	29.7	2.6	β-Zr

parameters expressed in nm differ in some cases on the second and on the third decimal number in other cases, in coincidence with the variations in the composition measurements between the as cast and the heat-treated samples.

Optical micrographs of heat treated samples at 900 °C are displayed in Fig. 1. $Zr_{45}Nb_{10}Fe_{45}$ sample (Fig. 1(a)) presents two different phases: λ_1 (wrinkled) and λ_2 (flat). $Zr_{40}Nb_{30}Fe_{30}$ sample (Fig. 1(b)) presents instead three different phases: the matrix (λ_2) and two phases of small size and different appearance, λ_1 (darker) and β-Zr. $Zr_{40}Nb_{50}Fe_{10}$ sample (Fig. 1(c)) also presents three phases, the λ_2 intermetallic (brighter zone) and two solid solutions, β-Zr and β-Nb (flatter areas).

On the other hand the $Zr_{61}Nb_{30}Fe_9$ sample (Fig. 1(d)) shows two phases, λ_2 and β-Zr. Finally the $Zr_{30}Nb_5Fe_{65}$ sample (Fig. 1(e)) presents only two phases (λ_2 and $(ZrNb)Fe_2$). The third one cannot be distinguished (Zr_2Fe) because is present in a scarce quantity.

4. Discussion

4.1. Laves phases

Laves phases are intermediate phases that can be obtained alloying elements with atomic diameters ratio $d_A/d_B = 1.225$ in the ideal case but there are cases where this relation varies between 1.1 and 1.6. They are topologically close-packed phases, particular atoms are surrounded by coordination polyhedra with 12–13–14–15 or 16 faces, presenting AB_2-type composition [12].

An important characteristic of this type of phases is the volume contractions associated to their formation. They crystallize in the following structure types: hexagonal $MgZn_2$-type (C14), cubic Cu_2Mg-type (C15) or hexagonal $MgNi_2$-type (C36).

Watson and Bennett [13] considered the occurrence of topologically close-packed (tcp) phases in terms of a volume factor and an electronic factor in binary transition-metal alloys. They determined that their approximation was better for Laves structures than for the rest of the tcp phases. In particular we are interested on how they placed the AB_2-type Laves structures on a map where a coordenate is the atomic volume ratio accounting for the volume contractions associated with compound formation and the other is a measure of the ***d***-band occupancy (N_h: average number of unoccupied states between the Fermi level and the top of the ***d***-bands).

On the other hand, Pettifor [14,15] proposed a pure phenomenological chemical scale χ, fixed to take the Pauling electronegativity values for Be through to F and defined to provide structural

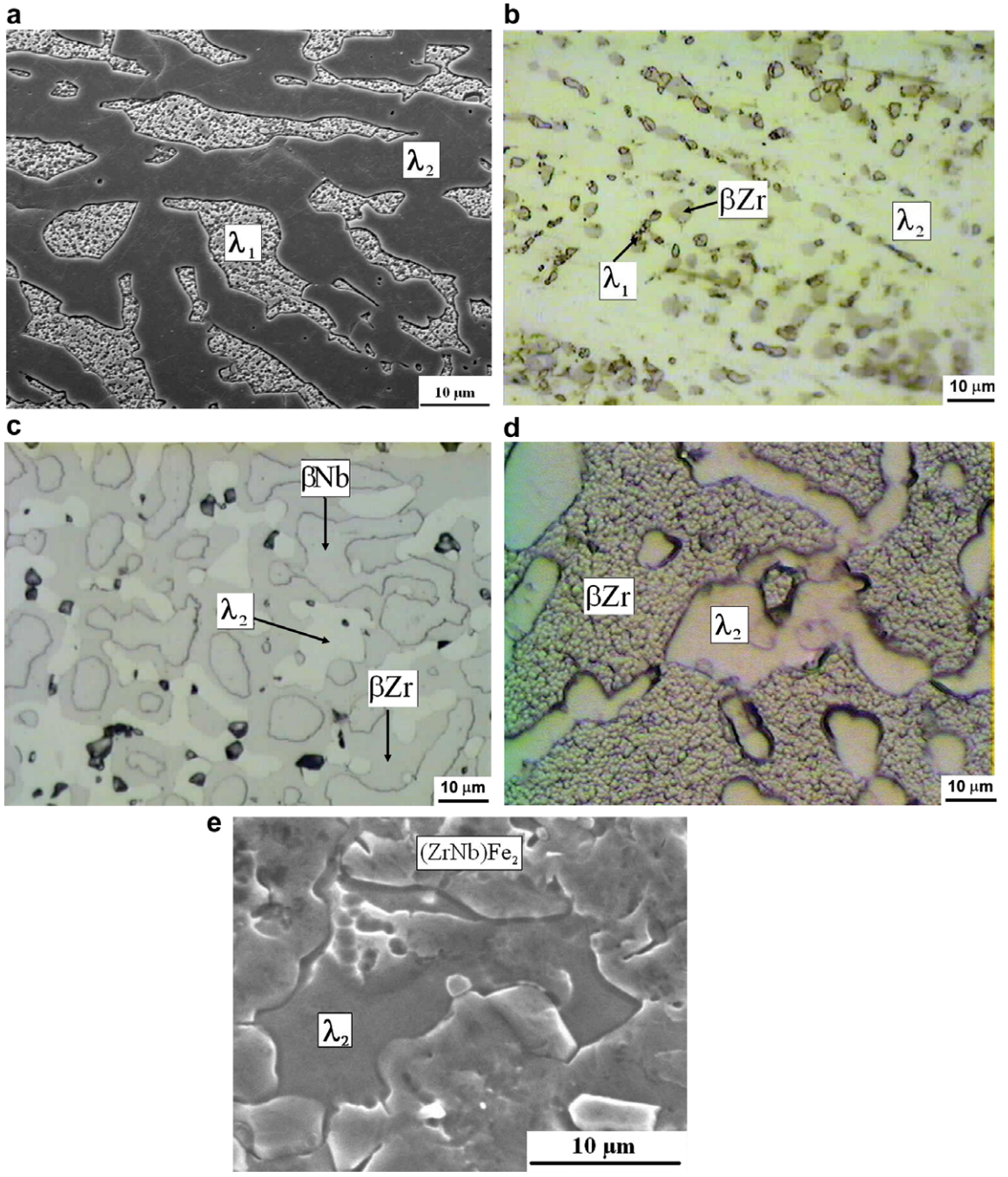

Fig. 1. (a) SEM micrograph of the $Zr_{45}Nb_{10}Fe_{45}$ sample, (b) optical micrograph of the $Zr_{40}Nb_{30}Fe_{30}$ sample, (c) optical micrograph of the $Zr_{40}Nb_{50}Fe_{10}$ sample, (d) optical micrograph of the $Zr_{61}Nb_{30}Fe_9$ sample, (e) SEM micrograph of the $Zr_{30}Nb_5Fe_{65}$ sample.

separation of binary compounds with a given stoichiometry A_xB_{1-x} in a single two-dimensional structural map (χ_A, χ_B). The predictive power of these maps comes from the fact that alloys with similar stable structures are grouped together. It is important to note that this phenomenological approximation does not provide an explanation to the origin of the different structural stability domains. The explanation could be found only by first principles calculations.

In the first part of a recent work by Stein et al. [16] various models for the prediction of the occurrence

and stability of Laves phases have been discussed, between them the Pettifor model, concluding that there is a lack in understanding the influence of the factors controlling the stability of Laves phases (atomic size, electronegativity and valence electrons). These authors do not consider Watson and Bennett maps, where another crucial factor is considered: the volume contractions associated to the compound formation.

The second part of Stein et al. work [17] presents examples from experimental investigations of binary and ternary intermetallic systems, showing the manifold possibilities how Laves phases may occur and the problems associated with their experimental verification.

4.2. λ_2 phase ($Zr(NbFe)_2$)

This is a ternary C14 Laves phase with hexagonal $MgZn_2$-type structure. At 900 °C has a wide range of compositions. Comparing the obtained values to our previous work [1–4] for alloys with variable compositions and considering that those values do not contradict values found in literature for precipitates of this phase in different Zr alloys [5,7,18–21], we could say that this phase would extend over the following composition range: $34 < \text{at.\% Zr} < 40$, $5 < \text{at.\% Nb} < 36$, $30 < \text{at.\% Fe} < 55$. Then, the lower existence range of this phase respecting the Fe content would be around 30 at.% Fe, 36 at.% Nb and 34 at.% Zr and the upper existence range respecting the Fe content would be around 55 at.% Fe, 5 at.% Nb and 40 at.% Zr. Note that this is a different range of compositions than that reported for the hexagonal C14-type $(ZrNb)Fe_2$ phase [2,6,8], showing that in the ternary Zr–Nb–Fe system there are two different hexagonal C14-type phases coming from different composition ranges of the diagram.

This is a well-known fact that the largest atoms in Laves phases usually occupy the 4f sites [22]. In the Zr–Nb–Fe system as the atomic radius of Zr (~0.160 nm) is the largest one, Zr would occupy this kind of sites while Fe and Nb atoms would be in the other positions. The Nb atomic radius (0.147 nm) is greater than the Fe atomic radius (0.127 nm), so Nb can probably occupy both A and B sites into the AB_2 Laves phase. The most probable mechanism in λ_2 phase is that of Fe substitution by Nb. In fact this consequence is also concluded considering the lattice parameters variation versus the Nb composition in the alloy. The lattice parameters increase linearly when Nb concentration increases (Table 2). This behavior coincides with Fe substitution by Nb and it is also evident from the values obtained by microanalysis measurements (Table 2). Finally it is also possible to verify it if we consider that the crystalline structure of this hcp phase is made of uniform spheres as close as it is possible. In that case the ideal ratio $c/a \sim 1.633$ would proceed. Considering the values obtained for the different compositions (Table 2) and seeing that $c/a > 1.633$ for the $Zr_{30}Nb_5Fe_{65}$ sample we can say that the λ_2 phase structure has compact planes of atoms piled up with a certain separation in this composition, in the others instead the c/a value is lower than the ideal one so there would be a compression due to the Fe atoms substitution by Nb atoms.

4.3. $(ZrNb)Fe_2$ phase

This is a ternary C15 Laves phase with $MgCu_2$-type structure that was detected in the heat treated at 900 °C $Zr_{30}Nb_5Fe_{65}$ sample, showing a composition of about $Zr_{25}Nb_5Fe_{70}$. The calculated lattice parameter was $a = 0.7029$ nm. Considering the Nb content in this phase, this value is consistent with that of the stoichiometric $ZrFe_2$ phase from the binary system Zr–Fe which is about 0.7075 nm for a sample heat-treated at 800 °C [23].

In the $ZrFe_2$ binary compound r_{Zr}/r_{Fe} is around 1.269, greater than the ideal ratio of atomic radii to form the AB_2 Laves phase (1.225). This is the reason for a region with a wide composition range in the binary Zr–Fe system. In the ternary case where Zr atoms are replaced by smaller Nb atoms (see microanalysis measurement from Table 2), r_A/r_B decreases becoming closer to the ideal value, then the solubility is favored only if the average ratio of atomic radii is not lower than the ideal ratio.

4.4. λ_2 and $(ZrNb)Fe_2$ occurrence

There are several binary and ternary systems with more than one Laves phase structure type. In [17] many examples of phase diagrams with composition-, temperature-, or pressure-dependent changes of the structure type are shown.

In the Zr–Nb–Fe case different Laves phases, $(ZrNb)Fe_2$ C15, C36 and C14-type and $Zr(NbFe)_2$ C14-type (λ_2) [6] for different compositions with homogeneity in wide composition ranges coexist. The $Zr_{30}Nb_5Fe_{65}$ sample is in a three phases region, two of them are Laves C14 (λ_2) and C15 ($(ZrNb)Fe_2$) phases. Something similar happens in

the Zr–Fe–Mo system [24] in which one the coexistence of Laves phases in the Fe-rich corner and in the center of the diagram is shown.

Considering Laves phases of the $A(B_xC_{1-x})_2$ and $(A_xB_{1-x})C_2$ types for different x values, the volume ratios were calculated and plotted. This way the presence of both λ_2 and $(ZrNb)Fe_2$ phases was checked by means of the predictive crystalline structure map of Watson and Bennett [13] extended to pseudobinaries by Granovsky [25].

Atomic volumes of each element were taken from [26] and the volumes per atom of the alloys were calculated from the lattice parameters for each structure and from the number of atoms per cell. For the C15 structure it was calculated as $a^3/24$ and for the hexagonal one as $3^{3/2}a^2c/72$. N_h values used were those given by Watson and Bennett [13].

In Fig. 2 the calculated values in the present work are plotted together with the values considered in [25] corresponding to 17 ternary systems with few exceptions which are also explained in [25]. In the specific case of the $(Zr_{1-x}Nb_x)Fe_2$ Laves phase the data to perform the calculations was obtained from Kanematsu [8]. This author reported a cubic C15-type structure for $x < 0.35$ and a hexagonal C14-type structure for $x > 0.5$. A good agreement with the model was observed including our result ($x = 0.17$) for the $Zr_{30}Nb_5Fe_{65}$ sample.

For the hexagonal C14-type $Zr(NbFe)_2$ phase, λ_2, our results also show a good agreement with the model, pointing out that this is a different C14-type phase from the C14-type $(Zr_{1-x}Nb_x)Fe_2$ for $x > 0.5$ mentioned above [8].

Moreover, in this work, an extended version to the Pettifor predictive model for pseudobinary systems with Laves structures of the $A(B_xC_{1-x})_2$ or $(A_xB_{1-x})C_2$ form was proposed by using χ_m as variable. This variable was calculated taking into account the phenomenological variable χ defined by Pettifor [14,15] for each chemical element (χ_A, χ_B or χ_C) in the alloy. Values were calculated as follows:

$$\chi_m(A) = \chi_A \quad \text{and} \quad \chi_m(B) = x\chi_B + (1-x)\chi_C, \quad \text{for } A(B_xC_{1-x})_2 \text{ structures}$$

$$\chi_m(B) = x\chi_A + (1-x)\chi_B \quad \text{and} \quad \chi_m(B) = \chi_C, \quad \text{for } (A_xB_{1-x})C_2 \text{ structures}$$

In Figs. 3 and 4 the corresponding maps constructed with the calculated values are shown. Laves phases appear separated rather well in cubic and hexagonal structures in this model, making a proper prediction of our experimental results.

4.5. β-Zr and β-Nb phases

It is important to note that in the ternary system Zr–Nb–Fe there are two regions of β phase which would correspond to the binary systems Zr–Nb and Zr–Fe [27,28]. The β phase in the Zr–Nb system at 900 °C presents a miscibility gap extending over the 40 < at.% Nb < 79 range [27]; on the other hand the solubility of Fe into the Nb–Fe system at 900 °C is approximately 1.5 at.% [29].

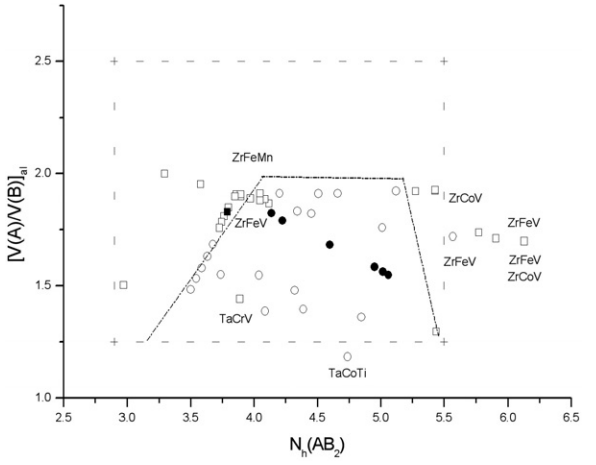

Fig. 2. Watson and Bennett Laves phases prediction model extension to pseudobinary systems [25]. (○) hexagonal structures, (●) hexagonal structures present work (λ_2 phase), (□) cubic structures, (■) cubic structures present work ((ZrNb)Fe_2 phase).

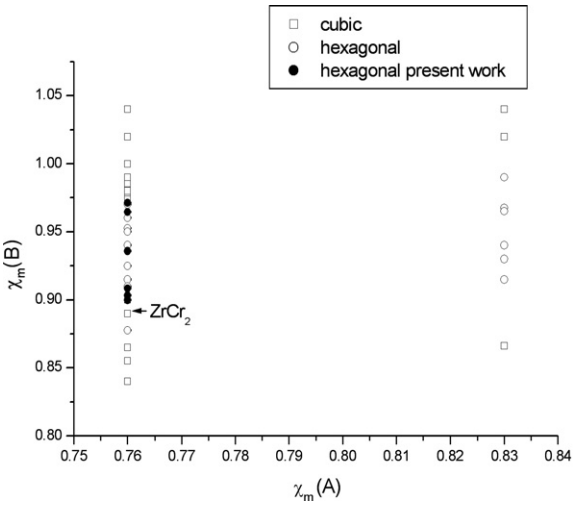

Fig. 3. Pettifor map, $\chi_m(A)$ vs. $\chi_m(B)$ for $A(B + C)_2$ compounds.

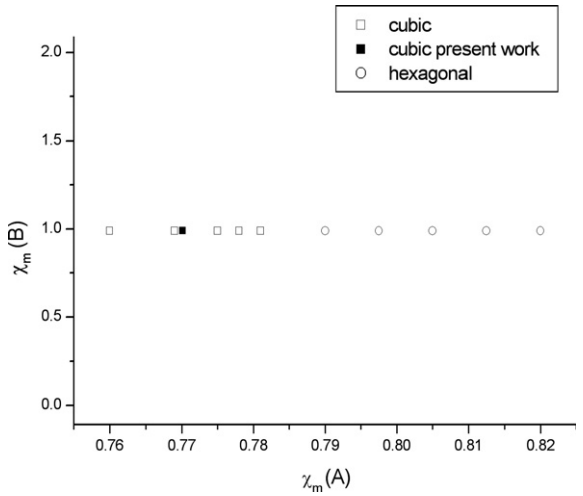

Fig. 4. Pettifor map, $\chi_m(A)$ vs. $\chi_m(B)$ for $(A + B)C_2$ compounds.

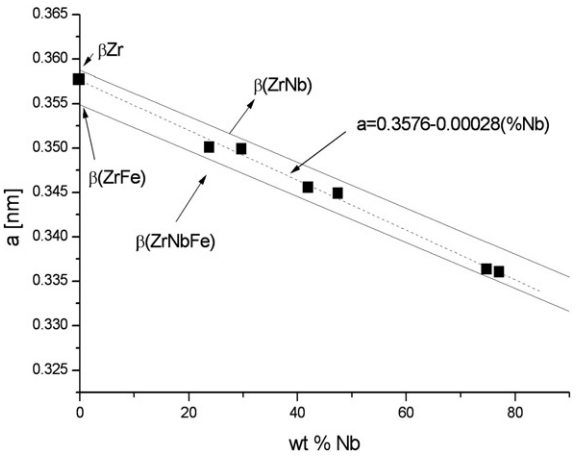

Fig. 5. Lattice parameter variation of the β phase with Nb concentration.

Taking into account the precedent data and considering our experimental results on the ternary system, the β-Zr phase would accept around up to 3 at.%. Fe in solid solution and would extend over the following range of compositions: 70 < at.% Zr < 97, 0 < at.% Nb < 30 and 0 < at.% Fe < 3. The β-Nb phase instead would accept up to 1.5 at.% Fe in solid solution and would extend over the following range of compositions: 0 < at.% Zr < 25, 75 < at.% Nb < 98.5 and 0 < at.% Fe < 1.5.

In the same way that there is a miscibility gap in the binary Zr–Nb system at 900 °C, from the present results it follows that the ternary system Zr–Nb–Fe at that temperature would also have a miscibility gap. This one would extend over the 25 < at.% Nb < 70 composition range, accepting around up to 3 at.% Fe.

If Vegard's law holds for a binary β(ZrNb) phase then the change in lattice parameter would be

$$a_{\beta(\mathrm{ZrNb})}(x) = a_{\beta\text{-Zr}} - (a_{\beta\text{-Zr}} - a_{\beta\text{-Nb}})x, \quad (1)$$

where x is the Nb concentration.

Generalizing this law for the ternary phase,

$$a_{\beta(\mathrm{ZrFeNb})}(x) = a_{\beta(\mathrm{ZrFe})} - (a_{\beta(\mathrm{ZrFe})} - a_{\beta\text{-Nb}})x. \quad (2)$$

Eqs. (1) and (2) are plotted in Fig. 5 together with the line obtained by interpolation of our results (dotted line), $a = 0.3576–0.00028$ (wt% Nb). The decreasing evolution of the lattice parameters with increasing Nb content in the phases due to Zr atoms substituted by Nb atoms (see also microanalysis measurements from Table 2), shows the increasing influence of Fe on the lattice parameter. A deviation from a random solid solution, as it is stated by Vegard's law, can be derived from Fig 5.

The same stabilization phenomenon with identical behavior happens for the β(ZrFe) phase with Ti incorporation [30].

Our results agree to a great extent with those of Cuello et al. [31] who studied the properties and stability of the bcc phase in the Zr–Nb system. They show the lattice parameter variation of the bcc phase in Zr–Nb alloys with different Nb contents including data from other authors.

4.6. λ_1 phase – $(ZrNb)_2Fe$

This cubic Ti_2Ni-type phase formed from the tetragonal Zr_2Fe intermetallic with Nb content greater than 0.5 at.% [1–4], presents a wide range of composition stability at 900 °C for the studied samples. Nb contents in this phase increase with Nb contents in the alloys.

Comparing the composition values obtained with previous works results and considering that there are no contradiction with values obtained in the literature for precipitates of this phase in different Zr alloys [5,19–21,32], we can say that it would extend over the following range of composition: 54 < at.% Zr < 64.5, 0.5 < at.% Nb < 16, 30 < at.% Fe < 35.

5. Conclusions

Conclusions can be summarized as follows:

– The a lattice parameter of the λ_2 phase varies between 0.5083 and 0.5344 nm and c varies

between 0.8315 and 0.8665 nm for the compositions studied in the present work, increasing linearly with Nb concentration, which indicates Fe substitution by Nb.

- The lower existence range with respect to the Fe content, taking into account the present work and previous works results [1–4], was about 30 at.% Fe, 34 at.% Zr and 36 at.% Nb and the upper one was about 55 at.% Fe, 5 at.% Nb and 40 at.% Zr for the λ_2 phase.
- In addition to the well-known Laves C15-type $(ZrNb)Fe_2$ phase (the polytypic C14 and C36 structures were not detected in the studied compositions), another Laves C14-type phase was found (λ_2: $Zr(NbFe)_2$). Watson and Bennett and also Pettifor structural maps helped to verify the occurrence of both of these phases.
- The lattice parameter a of the β phase changes linearly between 0.3360 and 0.3500 nm for the studied compositions.
- The Zr–Nb–Fe ternary system at 900 °C, as it happens in the binary Zr–Nb system, would have a miscibility gap (β-Zr + β-Nb) in the 25 < at.% Nb < 70 composition range, accepting up to 3 at.% Fe approximately.
- The composition range for the $(ZrNb)_2Fe$ phase, λ_1, taking into account the present work and previous works results [1–4], was around 54 < at.% Zr < 64.5, 0.5 < at.% Nb < 16, 30 < at.% Fe < 35.
- Finally a 900 °C section of the ternary (Zr–Nb–Fe) diagram in the studied region was proposed (Fig. 6), introducing some modifications to the last revision of the cited diagram [6].

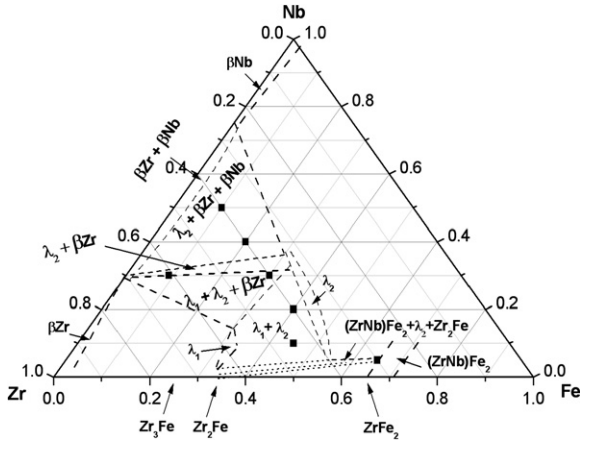

Fig. 6. 900 °C section proposal of the Zr–Nb–Fe phase diagram on the basis of the results obtained in the present work.

References

[1] C. Ramos, C. Saragovi, M. Granovsky, D. Arias, Hyperfine Interact. 122 (1999) 201.
[2] M.S. Granovsky, M. Canay, E. Lena, D. Arias, J. Nucl. Mater. 302 (2002) 1.
[3] C. Ramos, C. Saragovi, M. Granovsky, D. Arias, Hyperfine Interact. 139&140 (2002) 363.
[4] C. Ramos, C. Saragovi, M. Granovsky, D. Arias, J. Nucl. Mater. 312 (2003) 266.
[5] C. Toffolon-Masclet, P. Barberis, J.C. Brachet, J.P. Mardon, L. Legras, J. ASTM Int. 2(5) (2005), Paper ID: JAI12321, DOI: 10.1520/JAI12321.
[6] V. Raghavan, J. Phase Equilibr 24 (4) (2003) 354.
[7] O.T. Woo, G.J.C. Carpenter, in: 741 Proceedings of the XIIth International Congress for Electron Microscopy, AECL Report, 10264 (1990) 132.
[8] K. Kanematsu, J. Phys. Soc. Jpn. 27 (4) (1969) 849.
[9] C.P. Ramos, M.S. Granovsky, C. Saragovi, Physica B 389 (1) (2007) 67.
[10] M. Ruch, D. Arias, Scripta Metall. Mater. 24 (1990) 1577.
[11] L. Lutterotti, P. Scardi, J. Appl. Cryst. 25 (1992) 459.
[12] C. Barret, B. Massalski, Structure of Metals Crystallographic Methods, Principles, and Data, Mc Graw-Hill, 1966, p. 256.
[13] R.E. Watson, L.H. Bennett, Acta Metall. 32 (1984), p. 477, 491.
[14] D.G. Pettifor, Solid State Phys. 19 (1986) 285.
[15] D.G. Pettifor, Mater. Sci. Technol. 4 (1988) 675.
[16] F. Stein, M. Palm, G. Sauthoff, Intermetallics 12 (2004) 713.
[17] F. Stein, M. Palm, G. Sauthoff, Intermetallics 13 (2005) 1056.
[18] V.N. Shishov, A.V. Nikulina, V.A. Markelov, M.M. Peregud, A. Kozlov, S. Averin, S. Kolbenkov, A. Novoselov, in: Proceedings of the 11th International Symposium on Zirconium in the Nuclear Industry. ASTM STP, 1295 (1996), 603.
[19] C. Toffolon-Masclet, J.C. Brachet, C. Servant, L. Legras, D. Charquet, P. Barberis, J.P. Mardon, in: Proceedings of the 13th International Symposium on Zirconium in the Nuclear Industry, ASTM STP, 1423 (2002), 361.
[20] C. Toffolon-Masclet, J.C. Brachet, G. Jago, J. Nucl. Mater. 305 (2002) 224.
[21] P. Barberis, D. Charquet, V. Rebeyrolle, J. Nucl. Mater. 326 (2004) 163.
[22] W.B. Pearson, A Handbook of Lattice Spacings and Structures of Metals and Alloys, Pergamon, 1958, p. 657.
[23] G. Wiesinger, G. Hilscher, J. Phys. F: Met. Phys. 12 (1982) 497.
[24] M. Zinkevich, N. Mattern, Acta Mater. 50 (2002) 3373.
[25] M. Granovsky, Fases precipitadas en Zircaloy-4, Fases de Laveës, Tesis de Doctorado en Ciencias Físicas, Fac. Cs. Exactas, Univ. Nac. de La Plata, 1993.
[26] Atomic Size Parameters, Bulletin of Alloy Phase Diagrams, 2 (1982) 527.
[27] H. Okamoto, J. Phase Equilibr. 13 (5) (1992) 577.
[28] D. Arias, M.S. Granovsky, J.P. Abriata, Phase Diagrams of Binary Iron Alloys, in: H. Okamoto (Ed.), ASM International, Materials Park, OH, 1993, p. 467.
[29] H. Okamoto, J. Phase Equilibr 14 (5) (1993) 650.
[30] E. Galvão Da Silva, J.S. Coelho, R.A. Mansur, Acta Metall. 30 (1982) 1829.
[31] G.J. Cuello, A. Fernández Guillermet, G.B. Grad, R.E. Mayer, J.R. Granada, J. Nucl. Mater. 218 (1995) 236.
[32] V.V. Petkov, E.E. Cherkashin, Fiziko-teknichni ta matematichni nauki 32 (1972) 276.